Beamlets are Densely Embedded in H^{-1} *

Jianhong (Jackie) Shen
School of Mathematics, University of Minnesota, Minneapolis, MN 55455, USA
Lotus Hill Institute for Computer Vision and Information Science, E'Zhou, Wuhan 436000, China

Abstract

The insufficiency of using ordinary measurable functions to model complex natural images was first emphasized by David Mumford [31]. The idea was later rediscovered by Yves Meyer [29] who introduced proper texture models based on generalized functions or distributions. The simpler but effective Sobolev texture model of H^{-1} was subsequently explored by Osher, Sole, and Vese [34] to facilitate practical computation. H^{-1} textures have also been further employed in the recent works of Daubechies and Teschke [11], Lieu and Vese [25], Shen [39], and many others, leading to a new generation of models for image processing and analysis.

On the other hand, beamlets are the unconventional class of geometric wavelets invented by Donoho and Huo [14] to efficiently represent and detect lower dimensional singular image features. In the current work, we make an intriguing connection between the above two realms by demonstrating that H^{-1} is the natural space (of generalized functions) that hosts beamlets, and in return can be completely described by them. Computational evidences existing in the literature also help confirm this newly discovered bond.

Keywords: texture, oscillation, distribution, multiscale, singular measure, beamlets, beamlet expansion, Haar molecule, Haar potential, Poincaré-Sobolev inequality, grounded Poisson equation.

AMS Classification: 94A08, 42C40, 68U10.

1 Introduction

In this paper, an intriguing connection is established between two seemingly uncorrelated realms of developing works: the new generation of geometric wavelets - beamlets invented by Donoho and Huo [14, 15], and the more recent efforts of texture modeling using Sobolev distributions as initiated by Mumford [31], Meyer [29], and Osher, Sole, and Vese [34]. This newly discovered connection contributes to the the better understanding of some key questions in contemporary image analysis and processing:

[a] What are *typical* H^{-1}–textures? How do they *look* like generically as well as visually? What has one actually gained by going beyond *measurable* functions?

[b] Is there a classical analysis foundation for beamlets? Can such novel geometric entities still be accommodated in some suitable spaces of functions or distributions?

More specifically, in the current work we show that

*This work has been partially supported by the NSF (USA) under grant number DMS-0202565. Email: jhshen@math.umn.edu; Tel: (USA) (612) 625-3570.

[i] beamlets, as singular Radon measures in 2-D, can be naturally *embedded* in H^{-1}; and in return,

[ii] H^{-1} can be *completely* described by beamlets due to the denseness of beamlets, as well as a beamlet expansion formula in H^{-1}.

Our tools are mainly from real, functional, and classical wavelet analysis.

We now elaborate the background and motivations of the present work.

Image modeling stays at the very core of contemporary image processing and computer vision (see, e.g., [9, 31, 37, 46]), and provides the crucial regularity conditions for many illposed inverse problems in the fields [7]. Stochastically, images have been modelled as Markov or Gibbs random fields with coherent image structures that are discernable by well structured visual filters [20, 45, 46]. Deterministically or functionally, images have been modelled by function spaces including, for example, Sobolev spaces, Besov spaces in wavelet and multiresolution analysis [10, 12, 13, 16, 29], and the space of functions with bounded variations (BV) as first introduced into image restoration by Rudin, Osher, and Fatemi [2, 5, 6, 8, 35, 36, 38, 44]. Images from these spaces are all Lebesgue *measurable*, however.

In the late 1990's, Mumford (also see [31]) emphasized that the scaling characteristics observed from image statistics [18, 23] imply that measurable functions are *insufficient* tools for faithfully modeling complex natural images, and that *generalized* functions or *distributions* could serve better for this purpose. The idea was independently revived in the inspiring work of Meyer in 2001 [29] in which the theory of the so-called G-distributional textures was developed out of Rudin-Osher-Fatemi's image restoration model [36]. Subsequently, Osher, Sole, and Vese [34] further simplified the texture model by directly turning to the Sobolev distribution space H^{-1}, which is computationally more tractable than Meyer's. H^{-1}-textures have been further explored in the recent works of, for example, Daubechies and Teschke [11] using wavelets, Lieu and Vese [25] using even high order Sobolev distributions, Shen [39] for segmented image decomposition, and Aujol et al. [3, 4] for several sophisticated image processing tasks.

Despite all the new theoretical and computational degrees of freedom induced by Sobolev distributional textures, it has never been made clear in the literature as to *how such textures actually look like from the vision point of view, and what their most generic features are.* For example, in what sense can the popular texture samples sketched in Figure 1 be legitimately modelled and computed by H^{-1} distributions?

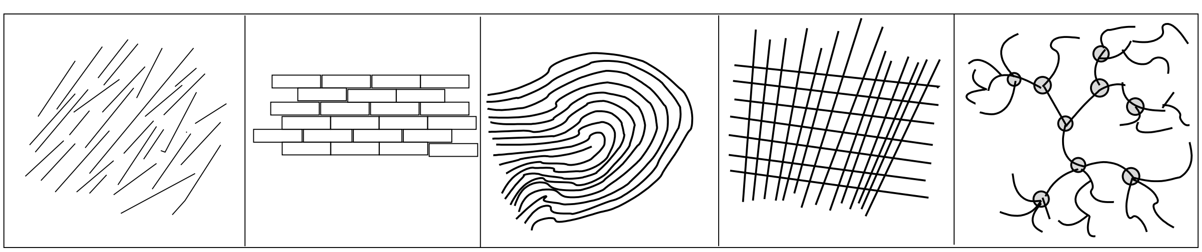

(a) straws (b) bricks (c) fingerprints (d) nets or fabrics (e) neurons

Figure 1: What do these typical textures (schematically drawn) have in common in image processing, computer graphics, and computer vision? They can all (i) be better *modelled* by H^{-1} distributions (as proposed by Osher, Sole, and Vese [34]) than by ordinary 2-D measurable functions , and (ii) be efficiently approximated by the beamlets of Donoho and Huo [14].

The theory of beamlets and beamlet decomposition, on the other hand, was developed by Donoho and Huo [14, 15] for a completely different purpose on signal detection.

From vision analysis, *lower-dimensional* image features in 2-D images are crucial visual cues for efficient scene interpretation. Well known examples include corners, T-junctions, and edges [22, 28, 33, 40]. 1-D image features, or curve-type of patterns, have played central roles in image and vision analysis since David Marr's early theory on edge detection [28].

There are two distinguishable categories of 1-D image features, or simply "curves" for convenience (in the sense of 1-D Hausdorff measure). The first class is often popularly referred to as "edges," along which 2-D image features (e.g., intensities, filter responses, etc.) experience noticeable jumps. This class serves the foundation for many existing works on edge detection and segmentation (e.g., [30, 32, 41, 42, 47]), and mathematically can be best modelled as the non-Cantor singular component of the total variation Radon measure $|Du|$ of a given BV image u [1, 2, 7, 21].

The other class of 1-D features comprise *isolated* curves or lines which are embedded in relatively *uniform* but often noisy backgrounds or *clutters*. Examples include the trajectories of basic particles in high-energy physics experiments, the branches of blood vessels or neurons (as in Figure 1), and the highways or watercourses in terrain images captured by spy planes or satellites. These isolated 1-D patterns are more difficult to capture even though trivial for the human vision. The fundamental challenge arises from the following dilemma:

"regular curves are of measure zero and thus negligible by the 2-D Lebesgue measure, while they are important cues for pattern formation and visual perception."

The framework and computational machinery of beamlets and beamlet decomposition were developed by Donoho and Huo [14, 15], to precisely meet this challenge, especially from the viewpoint of *signal detection theory.* A beamlet, is a line segment $\gamma = (A, B)$, from point A to B, as if a beam of light travels from A to B. This is the simple geometric definition but could disguise the *true* nature of a beamlet. According to the work of Donoho and Huo [14], we can conclude that a beamlet is really a 2-D singular Radon measure, so that for any test function $\phi \in \mathcal{D}(\Omega) = C_0^\infty(\Omega)$, one has the following signal response:

$$\langle \gamma, \phi \rangle = \int_\gamma \phi(z) ds,$$

where ds denotes the Euclidean length element along γ. That is, a beamlet is a *generalized* function or *distribution* in $\mathcal{D}'(\Omega)$, and must *not* be treated merely as a line segment with *finite* gray values along the pixels!

This is the point from which we make the connection between the above two realms of existing works: H^{-1} textures vs. the distributional view of beamlets, as well as make the contributions that have already been highlighted in the first paragraph. We show that the two, with completely different motivations to start with as briefly reviewed above, are in fact so intimately connected that they are almost identical to each other!

We must emphasize that the notation of beamlets, as employed in the current work, stays at this general level of functional analysis, and that we will not explore their rich properties (such as the dyadic beamlet dictionary and the tree-coding algorithm as in Figure 2) as fully developed by Donoho and Huo [14].

The organization of the rest of the paper goes as follows. Section 2 briefly reviews and develops some important properties of the space $H^{-1}(\Omega)$. Unlike many other works in existence, we rigorously work with a finite image domain Ω instead of $\mathbb{R}^2$. In Section 3, we introduce the more general notion of *color* beamlets, and show how they can be continuously embedded in $H^{-1}(\Omega)$. The embedding inequality is then further polished for a class of *boundary beamlets* on a simply connected image domain Ω, thanks to the *isoperimetric inequality.* In Section 4, we show that beamlets are dense in $H^{-1}(\Omega)$. Assisted with the classical Haar wavelets, we also establish a closed-form beamlet expansion formula for any H^{-1}-texture v on a square image domain. We emphasize that this beamlet expansion formula is different from that in Donoho and Huo for representing sparse curve features. The work concludes in Section 5.

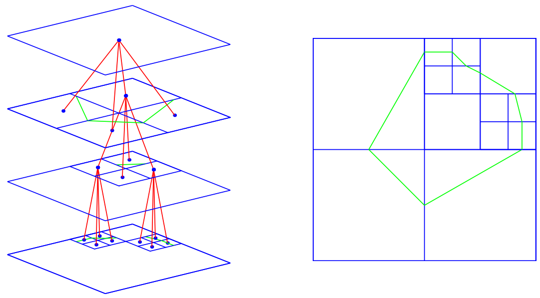

Figure 2: Multiscale beamlet decomposition via beamlet dictionaries and tree coding (from Donoho and Huo [14]).

2 The Texture Space $H^{-1}(\Omega)$

Let Ω be a bounded, simply connected, and open (image) domain in $\mathbb{R}^2$ which has a Lipschitz-continuous boundary manifold $\partial\Omega$. To avoid distractive but nonessential technicalities, we shall assume that Ω is regular enough (e.g., satisfying the *cone property* [17, 24]) so that the Poincaré or Sobolev types of inequalities hold on the domain.

Let $H^1(\Omega)$ denote the canonical Hilbert-Sobolev space of measurable functions on Ω of which each function element $u \in L^2(\Omega)$, and its distributional gradient $Du = \nabla u \in L^2(\Omega, \mathbb{R}^2)$. $H^1(\Omega)$ is naturally equipped with the Hilbert inner product:

$$\langle u,\, v\rangle_{H^1} = \int_\Omega uv + \int_\Omega \nabla u \cdot \nabla v,$$

where for simplicity the Lebesgue element $dx = dx_1 dx_2$ has been omitted in the integrals. The inner product then leads to the norm $\|u\|_{H^1} = \sqrt{\|u\|_{L^2}^2 + \|\nabla u\|_{L^2}^2}$.

$H_0^1(\Omega)$ is the subspace of $H^1(\Omega)$ comprising functions that have vanishing traces along $\partial\Omega$. Equivalently, $H_0^1(\Omega)$ is the closure (under the $\|\cdot\|_{H^1}$ norm) of all compactly supported C^∞ functions on Ω. For any $w(x) \in H_0^1(\Omega)$, the homogenenous semi-norm in H^1:

$$\|w\|_{H_0^1} = \|\nabla w\|_{L^2} = \left(\int_\Omega (\nabla w)^2\right)^{1/2},$$

is in fact tantamount to the norm $\|w\|_{H^1}$ according to Poincaré's inequality [17, 24]. Henceforth, we shall adopt this simpler norm structure for $H_0^1(\Omega)$, which corresponds to the inner product

$$\langle w,\, z\rangle = \langle w,\, z\rangle_{H_0^1} = \int_\Omega \nabla w \cdot \nabla z, \qquad \text{in} \quad H_0^1(\Omega).$$

Definition 1 **(H^{-1} Textures)** *The space $H^{-1} = H^{-1}(\Omega)$ is the dual space $\left(H_0^1\right)^*$, consisting of all linear functionals on H_0^1 that are continuous with respect to $\|\cdot\|_{H_0^1}$.*

Denote a typical element in H^{-1} by v or $\langle v,\, \cdot\rangle$, so that for any $w \in H_0^1$, the functional value $\langle v,\, w\rangle \in \mathbb{R}$ is linear in w and

$$|\langle v,\, w\rangle| \le C_v\, \|w\|_{H_0^1}, \quad \text{for some fixed constant } C_v.$$

The induced functional norm of v is thus given by

$$\|v\|_{H^{-1}} = \inf_{0 \neq w \in H_0^1} \frac{\langle v,\, w\rangle}{\|w\|_{H_0^1}}.$$

Proposition 1 *$\mathrm{div}(L^2(\Omega, \mathbb{R}^2)) \subseteq H^{-1}$, and for any $v = \nabla \cdot \boldsymbol{J}$, one has $\|v\|_{H^{-1}} \le \|\boldsymbol{J}\|_{L^2}$.*

Proof. For any flow field $\boldsymbol{J} \in L^2(\Omega, \mathbb{R}^d)$ and test function $\phi \in \mathcal{D}(\Omega) = C_0^\infty(\Omega)$, one has

$$|\langle \nabla \cdot \boldsymbol{J}, \phi \rangle| = |\langle \boldsymbol{J}, \nabla \phi \rangle| \le \|\boldsymbol{J}\|_{L^2} \cdot \|\nabla \phi\|_{L^2} = \|\boldsymbol{J}\|_{L^2} \cdot \|\phi\|_{H_0^1}.$$

Since H_0^1 is the completion of $\mathcal{D}(\Omega)$, $v = \nabla \cdot \boldsymbol{J}$ can be uniquely extended onto H_0^1, and

$$\langle v, w \rangle \le \|\boldsymbol{J}\|_{L^2} \cdot \|w\|_{H_0^1}, \qquad \text{for any} \qquad w \in H_0^1.$$

Thus, $v \in H^{-1}$, and $\|v\|_{H^{-1}} \le \|\boldsymbol{J}\|_{L^2}$. □

Proposition 2 (Riesz Representation) *For any texture $v \in H^{-1}$, there exists a unique "potential" function $\Phi \in H_0^1$, such that*

$$v = -\Delta \Phi \in \mathcal{D}'(\Omega), \qquad \textit{and} \qquad \|v\|_{H^{-1}} = \|\Phi\|_{H_0^1}.$$

Proof. By the Riesz-Hilbert representation theorem, for any $v \in H^{-1} = (H_0^1)^*$, there exists a unique $\Phi \in H_0^1$, such that for any $w \in H_0^1$,

$$\langle v, w \rangle = \langle \Phi, w \rangle_{H_0^1} = \int_\Omega \nabla \Phi \cdot \nabla w,$$

and $\|v\|_{H^{-1}} = \|\Phi\|_{H_0^1}$. Restricted on the test function space $w \in \mathcal{D}(\Omega) \subseteq H_0^1$, it is easy to see that v must be given by $v = -\Delta \Phi$ in the distributional sense after integration by parts. □

In combination, Proposition 1 and 2 lead to the following characterization theorem for H^{-1}.

Theorem 1 *One has $H^{-1}(\Omega) = \mathrm{div}(L^2(\Omega, \mathbb{R}^2))$, and for any $v \in H^{-1}$,*

$$\|v\|_{H^{-1}} = \inf_{\boldsymbol{J} : v = \nabla \cdot \boldsymbol{J}} \|\boldsymbol{J}\|_{L^2}.$$

The "minimum" flow $\boldsymbol{J}_v$ exists uniquely, and must be in the form of $\boldsymbol{J}_v = -\nabla \Phi$, for some unique $\Phi \in H_0^1$.

We briefly comment on the uniqueness of the minimum flow $\boldsymbol{J}_v$. It is trivial when $v = 0$, for which $\boldsymbol{J}_v = 0$. When $v \ne 0$, it is guaranteed by the general fact that *a Hilbert norm is always strictly convex on the non-zero level set of a linear map.* In our case, the linear map is the divergence operator.

3 Emerging of Beamlets in H^{-1} and Their Embedding

For any distribution $T \in \mathcal{D}'(\Omega)$, and any unit vector $\boldsymbol{b} \in S^1$, the directional derivative $\partial T / \partial \boldsymbol{b} \in \mathcal{D}'(\Omega)$ is defined by:

$$\left\langle \frac{\partial T}{\partial \boldsymbol{b}}, \phi \right\rangle = -\left\langle T, \frac{\partial \phi}{\partial \boldsymbol{b}} \right\rangle = -\langle T, \boldsymbol{b} \cdot \nabla \phi \rangle, \qquad \text{for any } \phi \in \mathcal{D}(\Omega).$$

Similarly, for any test flow field $\boldsymbol{J} = (J_1, J_2) \in \mathcal{D} \times \mathcal{D}$, one defines the vectorization $T \to T\boldsymbol{b}$ by:

$$\langle T\boldsymbol{b}, \boldsymbol{J} \rangle = \langle T, \boldsymbol{b} \cdot \boldsymbol{J} \rangle.$$

Then we must have:

$$\frac{\partial T}{\partial \boldsymbol{b}} = \mathrm{div}(T\boldsymbol{b}), \qquad \text{because for any } \phi \in \mathcal{D}, \quad \text{one has} \tag{1}$$

$$\left\langle \frac{\partial T}{\partial \boldsymbol{b}}, \phi \right\rangle = -\langle T, \boldsymbol{b} \cdot \nabla \phi \rangle = -\langle T\boldsymbol{b}, \nabla \phi \rangle = \langle \mathrm{div}(T\boldsymbol{b}), \phi \rangle.$$

Theorem 2 (New Characterization of H^{-1}) *We have*

$$H^{-1}(\Omega) = \text{span}\left\{ \frac{\partial f}{\partial \boldsymbol{b}} \ : \ f \in L^2(\Omega), \boldsymbol{b} \in S^1 \right\}, \tag{2}$$

and $\|\partial f/\partial \boldsymbol{b}\|_{H^{-1}} \leq \|f\|_{L^2}$.

Proof. By Theorem 1, for any $f \in L^2$ and $\boldsymbol{b} \in S^1$,

$$\frac{\partial f}{\partial \boldsymbol{b}} = \text{div}(f\boldsymbol{b}) \in \text{div}(L^2(\Omega, \mathbb{R}^2)) = H^{-1}(\Omega).$$

On the other hand, for any $v \in H^{-1}$, there exists some L^2 flow $\boldsymbol{J} = (f_1, f_2)$, such that $v = \text{div}(\boldsymbol{J})$. Then,

$$v = \frac{\partial f_1}{\partial x} + \frac{\partial f_2}{\partial y} = \frac{\partial f_1}{\partial \boldsymbol{e}_1} + \frac{\partial f_2}{\partial \boldsymbol{e}_2} \in \text{span}\left\{ \frac{\partial f}{\partial \boldsymbol{b}} \ : \ f \in L^2(\Omega), \boldsymbol{b} \in S^1 \right\},$$

where $\boldsymbol{e}_1 = (1, 0)$ and $\boldsymbol{e}_2 = (0, 1)$ are the two canonical orientations. Finally, by Proposition 1,

$$\|\frac{\partial f}{\partial \boldsymbol{b}}\|_{H^{-1}} \leq \|f\boldsymbol{b}\|_{L^2} = \|f\|_{L^2}, \qquad \text{since} \qquad \boldsymbol{b} \in S^1.$$

This completes the proof. $\square$

Definition 2 (Donoho and Huo's Beamlets) *A beamlet of Donoho and Huo on Ω is an open line segment $\gamma = (A, B) \subseteq \Omega$ with $A = (x_1, x_2)$ and $B = (y_1, y_2)$ in $\bar{\Omega}$, which leads to the distribution:*

$$\langle \gamma, \, \phi \rangle = \int_\gamma \phi(z) d\mathcal{H}^1. \tag{3}$$

Here $d\mathcal{H}^1$ denotes the 1-dimensional Hausdorff measure.

Definition 3 (Color Beamlets) *We define a color beamlet $\langle f|\gamma|$, with a pair of a beamlet γ and some function $f \in L^2(\gamma, d\mathcal{H}^1)$, to be the unique distribution in $\mathcal{D}'(\Omega)$ such that for any test function $\phi \in \mathcal{D}(\Omega)$,*

$$\langle f|\gamma|\phi \rangle = \int_\gamma f(z)\phi(z) d\mathcal{H}^1. \tag{4}$$

Here we have borrowed the bra-ket notation from Quantum Mechanics.

Therefore, an ordinary beamlet γ could be identified as the uniform color beamlet $\langle 1|\gamma|$.

Theorem 3 (Embedding of Color Beamlets in H^{-1}) *A color beamlet $\langle f|\gamma|$ must belong to $H^{-1}(\Omega)$, and*

$$\|\langle f|\gamma| \, \|_{H^{-1}} \leq C_\Omega \, \|f\|_{L^2(\gamma, d\mathcal{H}^1)},$$

for a universal constant C_Ω independent of f or γ.

Proof. Given a color beamlet $\langle f|\gamma|$, let $\boldsymbol{n}$ denote one of the two unit normals to γ. Define

$$\begin{aligned} E &= \{x = (x_1, x_2) \in \Omega \mid \text{for some } z \in \gamma, \ (x - z) \cdot \boldsymbol{n} = |x - z|\} \\ &= \{x \in \Omega \mid \text{for some } z \in \gamma \text{ and } t \geq 0, \ x = z + t\boldsymbol{n}\}. \end{aligned}$$

Extend f on γ to a function F on the entire image domain Ω by defining for any $x \in \Omega$,

$$F(x) = \begin{cases} 0, & x \notin E, \\ f(z), & x \in E \quad \text{and} \quad x = z + t\boldsymbol{n} \quad \text{for some } t \geq 0. \end{cases}$$

It is well defined since for any $x \in E$, the point z along γ is unique.

We then show that $F \in L^2(\Omega)$. Let $M = \operatorname{diam}(\Omega) < \infty$. Define

$$E_M = \{x = z + t\boldsymbol{n} \mid z \in \gamma, t \in [0, M]\} \subseteq \mathbb{R}^2,$$

and also define a function F_M on $\mathbb{R}^2$ by

$$F_M(x) = \begin{cases} 0, & x \notin E_M, \\ f(z), & x \in E_M \quad \text{and} \quad x = z + t\boldsymbol{n} \quad \text{for some } t \in [0, M]. \end{cases}$$

Then it is easy to see that $F_M\big|_\Omega = F$. Furthermore, by Fubini's Theorem [24],

$$\begin{aligned} \int_{\mathbb{R}^2} |F_M|^2 &= \int_{E_M} |F_M|^2 = \int_0^M dt \int_{\gamma + t\boldsymbol{n}} |F_M|^2 d\mathcal{H}^1 \\ &= \int_0^M dt \int_\gamma f(z)^2 d\mathcal{H}^1 = M \int_\gamma f^2 d\mathcal{H}^1. \end{aligned}$$

As a result,

$$\|F\|_{L^2(\Omega)} \leq \|F_M\|_{L^2(\mathbb{R}^2)} \leq \sqrt{M}\ \|f\|_{L^2(\gamma, d\mathcal{H}^1)}. \tag{5}$$

We now show that the color beamlet $\langle f|\gamma|$ is precisely $\partial F / \partial \boldsymbol{n}$. For any test function $\phi \in \mathcal{D}(\Omega)$,

$$\begin{aligned} \left\langle \frac{\partial F}{\partial \boldsymbol{n}}, \phi \right\rangle &= -\langle F, \boldsymbol{n} \cdot \nabla \phi \rangle = -\int_E F \frac{\partial \phi}{\partial \boldsymbol{n}} dx \\ &= -\int_E F(z + t\boldsymbol{n}) \frac{\partial \phi}{\partial t}(z + t\boldsymbol{n}) dt d\mathcal{H}^1(z) \\ &= -\int_\gamma f(z) d\mathcal{H}^1(z) \int_{L_z} \frac{\partial}{\partial t} \phi(z + t\boldsymbol{n}) dt \\ &= \int_\gamma f(z)\phi(z) d\mathcal{H}^1(z) = \langle f|\gamma|\phi\rangle. \end{aligned} \tag{6}$$

Here for each $z \in \gamma$, L_z denotes the ensemble of line segments (possibly more than one) which are the intersection of $z + \mathbb{R}^+\ \boldsymbol{n}$ with Ω. Notice that all the endpoints in L_z must belong to $\partial\Omega$ except for z, which belongs to $\gamma \subseteq \Omega$, and also notice that $\phi \in \mathcal{D}(\Omega)$ vanishes along $\partial\Omega$.

Finally, in combination of (6), (5), and Theorem 2, one has

$$\| \langle f|\gamma|\, \|_{H^{-1}} = \| \frac{\partial F}{\partial \boldsymbol{n}} \|_{H^{-1}} \leq \|F\|_{L^2} \leq C_\Omega \|f\|_{L^2(\gamma, d\mathcal{H}^1)},$$

where $C_\Omega \leq \sqrt{M} = \sqrt{\operatorname{diam}(\Omega)}$. This completes the proof. □

Corollary 1 (Square Root Bound) *Let $\gamma = \langle 1|\gamma|$ be a canonical beamlet of Donoho and Huo in Ω. Then*

$$\|\gamma\|_{H^{-1}} \leq C_\Omega\ \sqrt{|\gamma|},$$

where $|\gamma|$ denotes the Euclidean length and C_Ω is a constant independent of γ.

Remarkably, this square-root scaling law was already employed in the original work of Dohono and Huo [14] for designing normalized comparable statistics.

Definition 4 (Boundary Beamlets) *A beamlet γ is said to be a boundary beamlet if $\partial\gamma \subseteq \partial\Omega$, i.e., the two endpoints belong to the boundary of the image domain.*

We now show that for boundary beamlets, the above square-root bound can be further improved (for the limit when the length $|\gamma| \to 0$).

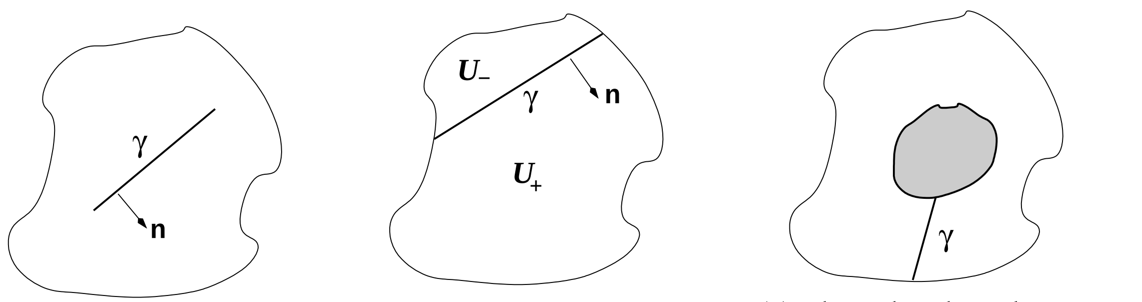

(a) a typical beamlet (b) a boundary beamlet (c) a boundary beamlet on a non−simply connected domain

Figure 3: Left: a general beamlet γ and its normal $\boldsymbol{n}$ (for the proof of Theorem 3); Middle: a *boundary* beamlet γ partitions a simply connected image domain Ω into two disjoint open sets $U_\pm$ (for the proof of Theorem 4); Right: if the domain is not simply connected, the situation depicted in the middle could fail to occur.

Theorem 4 (Sharper Bound for Boundary Beamlets) *There exists some constant $C > 0$ which is even independent of Ω, such that for any boundary beamlet γ, one has*

$$\|\gamma\|_{H^{-1}} \leq C\,|\gamma|.$$

Proof. Since Ω is bounded, simply connected, and has a Lipschitz continuous boundary $\partial\Omega$, $\partial\Omega$ must be a Jordan simple curve and is segmented into two disjoint segments by $\partial\gamma$. Joined by the given boundary beamlet γ, each segment circumvents an open subdomain of Ω. Denote the two subdomains by U_+ and U_-, and their characteristic functions by χ_+ and χ_- (see Figure 3).

Let $\boldsymbol{n}$ denote any one of the two unit normals of γ. Then as in the proof of the preceding theorem, one has in H^{-1},

$$\gamma = \langle 1|\gamma| = \pm\frac{\partial\chi_\pm}{\partial\boldsymbol{n}}.$$

By Theorem 2, one has (with $a \wedge b = \min(a, b)$),

$$\|\gamma\|_{H^{-1}} \leq \|\chi_+\|_{L^2} \wedge \|\chi_-\|_{L^2},$$

or equivalently,

$$\|\gamma\|_{H^{-1}} \leq \sqrt{|U_+| \wedge |U_-|}, \qquad \text{with } |U| \text{ denoting the 2-D Lebesgue measure of } U \subseteq \Omega. \tag{7}$$

Let $\langle f\rangle$ denote the average of any measurable function f on Ω:

$$\langle f\rangle = \frac{1}{|\Omega|}\int_\Omega f(x)dx.$$

Then by the Poincaré-Sobolev inequality, or the generalized isoperimetric inequality [17, 21], there exists a constant $\tilde{C} > 0$ which is independent of Ω in 2-D, such that

$$\|\chi_+ - \langle \chi_+ \rangle\|_{L^2(\Omega)} \le \tilde{C}\, |D\,\chi_+|(\Omega), \tag{8}$$

where the *total variation* Radon measure is given by $|D\,\chi_+|(\Omega) = |\gamma|$ due to the construction of U_+. On the other hand, one has

$$\begin{aligned} \|\chi_+ - \langle \chi_+ \rangle\|^2_{L^2(\Omega)} &= \int_{U_+} \left(1 - \frac{|U_+|}{|\Omega|}\right)^2 + \int_{U_-} \left(\frac{|U_+|}{|\Omega|}\right)^2 \\ &= \left(1 - \frac{|U_+|}{|\Omega|}\right)^2 |U_+| + \left(\frac{|U_+|}{|\Omega|}\right)^2 |U_-| \\ &= \frac{|U_+| \cdot |U_-|}{|\Omega|} \ge \frac{1}{2}\, |U_+| \wedge |U_-|, \end{aligned} \tag{9}$$

where the last inequality is universal for any two reals a and b:

$$\frac{1}{2}\, a \wedge b \le \frac{a \cdot b}{a + b} \le a \wedge b.$$

Finally, the combination of (9), (8), and (7) leads to

$$\|\gamma\|_{H^{-1}} \le C|\gamma|, \qquad \text{with } C = \sqrt{2}\, \tilde{C} \text{ independent of } \Omega.$$

This completes the proof. □

Notice that the above improvement has been made possible due to the construction of $H^{-1}(\Omega)$, which is the dual of $H^1_0(\Omega)$. H^{-1}-textures are hence less "expensive" along or near $\partial\Omega$ since the sensors in $H^1_0(\Omega)$ vanish along $\partial\Omega$. In terms of computer or human vision, this implies that an observer focuses the attention in the interior of Ω, and blurs or filters out the details towards the boundary of the visual field Ω.

4 Denseness of Beamlets in H^{-1}; Beamlet Decomposition

In this section, we show that beamlets are actually a *complete* class of representatives in H^{-1}.

4.1 Denseness of Beamlets in H^{-1}

For a given beamlet γ and any scalar $c \in \mathbb{R}$, we shall use the notation $c\gamma$ to denote the color beamlet $\langle c|\gamma|$, so that

$$\langle c\gamma, \phi \rangle = \langle c|\gamma|\phi \rangle = c \int_\gamma \phi d\mathcal{H}^1, \qquad \text{for any test function } \phi \in \mathcal{D}(\Omega).$$

If c is a positive integer, then as in the geometric measure theory of varifolds [26], we can call c the *multiplicity* of γ.

Theorem 5 (Denseness of Beamlets in H^{-1}) *We have*

$$H^{-1}(\Omega) = \text{closure}\{\text{span}\{\textit{beamlets in } \Omega\}\}.$$

That is, for any $v \in H^{-1}(\Omega)$ and $\varepsilon > 0$, there exist a finite collection of beamlets $\{\gamma_n \mid n = 1 : N\}$ and coefficients $\{c_n \mid n = 1 : N\}$, such that

$$\|v - \sum_{n=1}^N c_n \gamma_n\|_{H^{-1}} \le \varepsilon. \tag{10}$$

Proof. For any integer j, let D_j denote the ensemble of dyadic cubes in $\mathbb{R}^2$ at scale 2^{-j}:

$$D_j = \{2^{-j}(k + (0,1) \times (0,1)) \ : \ k = (k_1, k_2) \in \mathbb{Z}^2\}, \qquad j = \cdots, -1, 0, 1, \cdots.$$

For a given bounded image domain Ω, further define

$$D_j(\Omega) = \{Q \in D_j \mid Q \subseteq \Omega\}, \qquad \text{and} \qquad F_j(\Omega) = \mathrm{span}\{\chi_Q(x) \mid Q \in D_j(\Omega)\}.$$

Then by the classical real analysis of L^2 [19, 24], one has

$$F_j(\Omega) \subseteq F_{j+1}(\Omega), \qquad \text{and} \qquad L^2(\Omega) = \mathrm{closure}\left(\lim_{j\to+\infty} F_j(\Omega)\right). \tag{11}$$

Since $H^{-1} = \mathrm{div}(L^2(\Omega, \mathbb{R}^2)) = \left\{v = \dfrac{\partial f}{\partial x} + \dfrac{\partial g}{\partial y} \;\Big|\; f, g \in L^2(\Omega)\right\}$, it suffices to establish (10) for v's in the form of $\partial f/\partial x$ or $\partial g/\partial y$. Take $v = \partial f/\partial x$ for example. By (11), for any $\varepsilon > 0$, there exist some resolution level j, some coefficients $c_{1:N}$, and some cubes $Q_{1:N}$ in $D_j(\Omega)$, such that

$$\|f - \sum_{n=1}^{N} c_n \chi_{Q_n}\|_{L^2} \leq \varepsilon.$$

Then one has

$$\|v - \sum_{n=1}^{N} c_n \frac{\partial}{\partial x}\chi_{Q_n}\|_{H^{-1}} \leq \|f - \sum_{n=1}^{N} c_n \chi_{Q_n}\|_{L^2} \leq \varepsilon. \tag{12}$$

On the other hand, assume $Q_n = (a_n, b_n) \times (c_n, d_n)$, and define two vertical side beamlets:

$$\gamma_n^+ = \{b_n\} \times (c_n, d_n), \qquad \text{and} \qquad \gamma_n^- = \{a_n\} \times (c_n, d_n).$$

Then in H^{-1}, one has

$$\frac{\partial}{\partial x}\chi_{Q_n} = \langle -1|\gamma_n^+| + \langle 1|\gamma_n^-| = -\gamma_n^+ + \gamma_n^-,$$

and (12) yields the desired beamlets approximation in H^{-1}:

$$\|v - \sum_{n=1}^{N} c_n(\gamma_n^- - \gamma_n^+)\|_{H^{-1}} \leq \varepsilon. \tag{13}$$

This completes the proof. $\square$

More specifically, for any cube Q, let $\partial^* Q$ denote its four side beamlets. For any scale j, define the ensemble of all such side beamlets at scale j by

$$B_j(\Omega) = \bigcup_{Q \in D_j(\Omega)} \partial^* Q.$$

Then based on (13) (and a similar formula for $v = \partial g/\partial y$), one can easily prove the following corollary.

Corollary 2 *For any scale $j \in \mathbb{Z}$, one has (in $H^{-1}(\Omega)$)*

$$B_j(\Omega) \subseteq \mathrm{span}\{B_{j+1}(\Omega)\}, \qquad \textit{and} \qquad H^{-1}(\Omega) = \mathrm{closure}\left(\lim_{k\to+\infty} \mathrm{span}\{B_k(\Omega)\}\right).$$

Next we show that a multiscale beamlet decomposition formula is possible in $H^{-1}(\Omega)$ when Ω is a rectangular image domain. After normalization one can assume that the image domain Ω is the unit square $\Omega = (0,1) \times (0,1)$.

4.2 Haar's Orthonormal Wavelet System on Ω

As in the classic wavelet theory [10, 27, 43], define the *template* Haar scaling function and wavelet on the unit interval $(0,1)$ by:

$$h_0(s) = 1_{(0,1)}(s), \qquad \text{and} \qquad h_1(s) = 1_{(0,\,1/2)}(s) - 1_{[1/2,\,1)}(s),$$

which in the multiresolution framework lead to an orthonormal wavelet expansion of $L^2(0,1)$. By tensor product, they induce the 2-D template Haar scaling function and three wavelets on Ω:

$$h_\alpha(x) = h_{(t_1,\,t_2)}(x_1, x_2) = h_{t_1} \otimes h_{t_2} = h_{t_1}(x_1)\, h_{t_2}(x_2),$$

with the type index $\alpha = (t_1, t_2) \in \{(0,0),\ (1,0),\ (0,1),\ (1,1)\} = \Lambda$. For convenience, also define the wavelet type-index set

$$\Lambda^* = \{\ (1,0),\ (0,1),\ (1,1)\},$$

which correspond to the horizontal, vertical, and diagonal oscillations, separately.

Let I denote a generic dyadic subcell of Ω so that

$$I \in \mathcal{B} = \left\{2^{-j} \cdot \{(k_1, k_1+1) \times (k_2, k_2+1)\} \ :\ j = 0, 1, \cdots, \text{ and } k_1, k_2 \in \{0, 1, \cdots, 2^j - 1\}\right\}.$$

That is, associated with the cell symbol I is a unique pair of data: resolution level j, and the location of the lower left corner $2^{-j}(k_1,\ k_2)$ of the square cell. Symbolically, one can thus identify I with the triple $(j; k_1, k_2)$. For each dyadic cell $I \in \mathcal{B}$ and wavelet type-index $\alpha \in \Lambda^*$, define the associated Haar wavelet $h_{\alpha,I}(x)$ by:

$$h_{\alpha,I}(x) = h_{\alpha,I}(x_1, x_2) = 2^j h_\alpha\left(2^j x_1 - k_1, 2^j x_2 - k_2\right).$$

Then the following is a well known theorem in wavelet theory [10, 43].

Proposition 3 *Together with the template Haar scaling function $h_{\alpha=(0,0)}(x)$, the Haar wavelets*

$$\{h_{\alpha,I}(x) \mid \alpha \in \Lambda^*,\ I \in \mathcal{B}\}$$

consist into an orthonormal basis for $L^2(\Omega)$.

4.3 Haar Molecules of Beamlets and Haar Potentials

Based on the classic Haar wavelets, we now introduce the notion of *Haar molecules* of beamlets. As in chemistry, here a molecule refers to a *specific* configuration of finitely many individual beamlets (or atoms).

Definition 5 (Haar Molecules of Beamlets) *For each Haar wavelet $h_{\alpha,I}(x)$, define two associated Haar molecules of beamlets by:*

$$b^{(1)}_{\alpha,I} = \frac{\partial}{\partial x_1} h_{\alpha,I}(x_1, x_2), \qquad \textit{and} \qquad b^{(2)}_{\alpha,I} = \frac{\partial}{\partial x_2} h_{\alpha,I}(x_1, x_2).$$

Proposition 4 *For each $i \in \{1,2\}, \alpha \in \Lambda^*$, and $I \in \mathcal{B}$, the Haar molecule (see Figure 4)*

$$b^{(i)}_{\alpha,I} \in \mathrm{span}\{\textit{beamlets in } \Omega\}.$$

Proof. Due to the scaling and translation similarities, it suffices to prove the claim for the template wavelets when $I = (j = 0; k_1 = 0, k_2 = 0)$. Take type $\alpha = (1, 1)$ and $i = 1$ for example. By definition, as well as Dirac's delta function, one has

$$\begin{aligned}
b^{(1)}_{(1,1)} &= \frac{\partial}{\partial x_1} h_{(1,1)}(x) = h_1(x_2) \times \frac{\partial}{\partial x_1} h_1(x_1) \\
&= \left(1_{(0,\,1/2)}(x_2) - 1_{(1/2,\,1)}(x_2)\right) \times \frac{\partial}{\partial x_1}\left(1_{(0,\,1/2)}(x_1) - 1_{(1/2,\,1)}(x_1)\right) \\
&= \left(1_{(0,\,1/2)}(x_2) - 1_{(1/2,\,1)}(x_2)\right) \times \left(\delta(x_1) - 2\delta(x_1 - 1/2) + \delta(x_1 - 1)\right) \\
&= \gamma_{0,0} - \gamma_{0,1} - 2\gamma_{1/2,\,0} + 2\gamma_{1/2,\,1} + \gamma_{1,0} - \gamma_{1,1},
\end{aligned} \tag{14}$$

where the six beamlets in the last step are given by

$$\gamma_{s,0} = \{s\} \times (0,\ 1/2), \qquad \text{and} \qquad \gamma_{s,1} = \{s\} \times (1/2,\ 1), \qquad s = 0, 1/2, 1.$$

The last step of beamlet representation has been made possible by the general equivalence:

$$\begin{aligned}
\int_\Omega \delta(x_1 - s) f(x_2)\phi(x) dx_1 dx_2 &= \int_0^1 f(x_2) dx_2 \int_0^1 \phi(x_1, x_2))\delta(x_1 - s) dx_1 \\
&= \int_0^1 f(x_2)\phi(s, x_2) dx_2 = \int_{\gamma_s} f(z)\phi(z) d\mathcal{H}^1(z),
\end{aligned}$$

for any $f \in L^2(0, 1)$, $s \in (0, 1)$, test function $\phi(x) \in \mathcal{D}(\Omega)$, and the beamlet $\gamma_s = \{s\} \times (0, 1)$. Thus the generalized function $v = \delta(x_1 - s)f(x_2)$ can always be identified with the color beamlet $\langle f|\gamma_s|$. On the other hand, a piecewise constant color beamlet is apparently spanned by ordinary beamlets. Other cases of α and i can be proven similarly. This completes the proof. $\square$

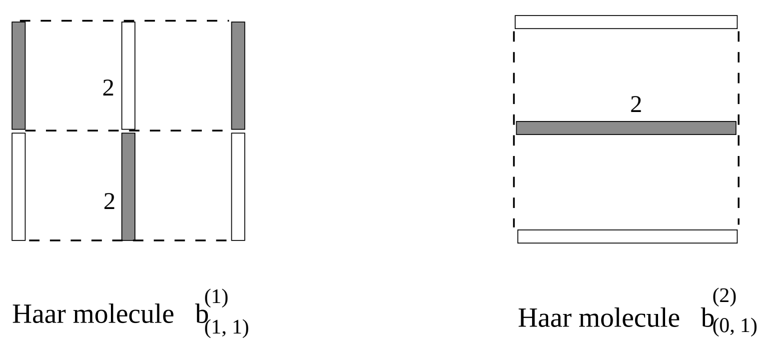

Figure 4: Left: the Haar molecule $b^{(1)}_{(1,1)}$ consisting of 6 vertical beamlets half of which are negative (shaded bars). Right: another Haar molecule $b^{(2)}_{(0,1)}$. The number beside a beamlet denotes its multiplicity (or color) in the molecule (see the last expression in Eqn. (14)). Pay attention to the *oscillatory* nature of these generic molecules, which is known to be important in texture modeling.

Definition 6 (Haar Potentials) *For each Haar molecule $b^{(i)}_{\alpha,I}$ with $i \in \{1, 2\}, \alpha \in \Lambda^*$, and $I \in \mathcal{B}$, we define the associated Haar potential $B^{(i)}_{\alpha,I}$ to be the unique element in $H^1_0(\Omega)$ which solves the grounded Poisson equation in the distributional sense:*

$$-\Delta B^{(i)}_{\alpha,I} = b^{(i)}_{\alpha,I}, \text{ on } \Omega; \qquad \text{and} \qquad B^{(i)}_{\alpha,I}\big|_{\partial\Omega} = 0.$$

4.4 Beamlet Expansion in H^{-1} via Haar Molecules

Theorem 6 *Let $\langle\cdot,\,\cdot\rangle$ denote the dual action of H^{-1} and H_0^1 on the unit square domain Ω. Then for any $v \in H^{-1}(\Omega)$, one has the following beamlet expansion via Haar molecules and Haar potentials:*

$$v = \sum_{i\in\{1,2\},\alpha\in\Lambda^*,I\in\mathcal{B}} \left\langle v,\, B_{\alpha,I}^{(i)} \right\rangle\, b_{\alpha,I}^{(i)}, \tag{15}$$

which converges strongly in the norm of H^{-1}.

Proof. By Riesz representation in Proposition 2, given $v \in H^{-1}$, let $\Phi \in H_0^1$ denote the potential of v which solves the grounded Poisson equation in the distributional sense:

$$-\Delta\Phi = v, \qquad \text{on } \Omega, \qquad \text{and} \qquad \Phi\big|_{\partial\Omega} = 0.$$

Then $\boldsymbol{J} = -\nabla\Phi = (-\Phi_{x_1},\, -\Phi_{x_2}) \in L^2(\Omega, \mathbb{R}^2)$, and one has the Haar wavelet expansion:

$$-\Phi_{x_i} = \sum_{\alpha\in\Lambda^*,I\in\mathcal{B}} \langle -\Phi_{x_i},\, h_{\alpha,I}\rangle\; h_{\alpha,I}, \qquad i = 1, 2.$$

Notice that since $\displaystyle\int_\Omega \Phi_{x_i}(x)dx = 0$, the wavelet expansion does not need to include the ordinary term of $\langle -\Phi_{x_i}\rangle$ at the coarsest scale $j = 0$.

Since div : $L^2(\Omega, \mathbb{R}^2) \to H^{-1}$ is a continuous operator according to Proposition 1, from the L^2 infinite series one arrives at:

$$\begin{aligned} v = \operatorname{div}(\boldsymbol{J}) &= \sum_{i=1,2} (-\Phi_{x_i})_{x_i} \\ &= \sum_{\alpha\in\Lambda^*,I\in\mathcal{B}} \sum_{i=1,2} \langle -\Phi_{x_i},\, h_{\alpha,I}\rangle\; \frac{\partial}{\partial x_i} h_{\alpha,I} \\ &= \sum_{i\in\{1,2\},\alpha\in\Lambda^*,I\in\mathcal{B}} \langle -\Phi_{x_i},\, h_{\alpha,I}\rangle\; b_{\alpha,I}^{(i)}. \end{aligned} \tag{16}$$

On the other hand,

$$\begin{aligned} \langle -\Phi_{x_i},\, h_{\alpha,I}\rangle &= \left\langle \Phi,\, (h_{\alpha,I})_{x_i} \right\rangle = \left\langle \Phi,\, b_{\alpha,I}^{(i)} \right\rangle \\ &= \left\langle \Phi,\, -\Delta B_{\alpha,I}^{(i)} \right\rangle = \left\langle -\Delta\Phi,\, B_{\alpha,I}^{(i)} \right\rangle = \left\langle v,\, B_{\alpha,I}^{(i)} \right\rangle. \end{aligned}$$

In combination with (16), this leads to the molecular beamlet expansion:

$$v = \sum_{i\in\{1,2\},\alpha\in\Lambda^*,I\in\mathcal{B}} \left\langle v,\, B_{\alpha,I}^{(i)} \right\rangle\, b_{\alpha,I}^{(i)}.$$

The infinite series converges strongly in H^{-1}, which concludes the proof. □

In terms of imaging and signal analysis, the above beamlet expansion has a clear meaning. For any given H^{-1} texture or signal v, in order to perceive its projection or reaction to a Haar molecule $b_{\alpha,I}^{(i)}$, one has to apply the smoother Haar potential $B_{\alpha,I}^{(i)}$ of that molecular to *probe* the signal (i.e., via $\left\langle v,\, B_{\alpha,I}^{(i)} \right\rangle$).

Theorem 6 or the expansion formula (15) may have suggested that the Haar molecules and Haar potentials consist into a *biorthogonal* system [10, 43]. This is, however, not the case because of the non-commutativity between $\partial/\partial x_i$'s and $(-\Delta)^{-1}$ due to the grounded boundary condition.

5 Conclusion

In the current work, an intriguing connection has been made between the H^{-1} texture model first proposed by Osher, Sole, and Vese [34] (and also subsequently developed by many others), and the nonconventional generation of geometric wavelets called beamlets first developed by Donoho and Huo [14, 15]. The most striking discovery for these seemingly uncorrelated realms can be summarized into one sentence: *beamlets are densely embedded in and hence can completely describe H^{-1} textures.*

Thus on one hand, our work has discovered the natural functional space that accommodates the untraditional wavelets - beamlets, and on the other hand, the work answers the crucial questions at the heart of contemporary variational texture modeling - "how does a *typical* H^{-1}–texture pattern look like, and how can one synthesize such a typical example when requested?" This unexpected theoretical bond has also been confirmed by the existing computational results such as the one in Figure 5 from Shen [39].

We also wish that the current work could inspire a newer look at the original works of Donoho and Huo [14, 15] on beamlet modeling, analysis, and computation.

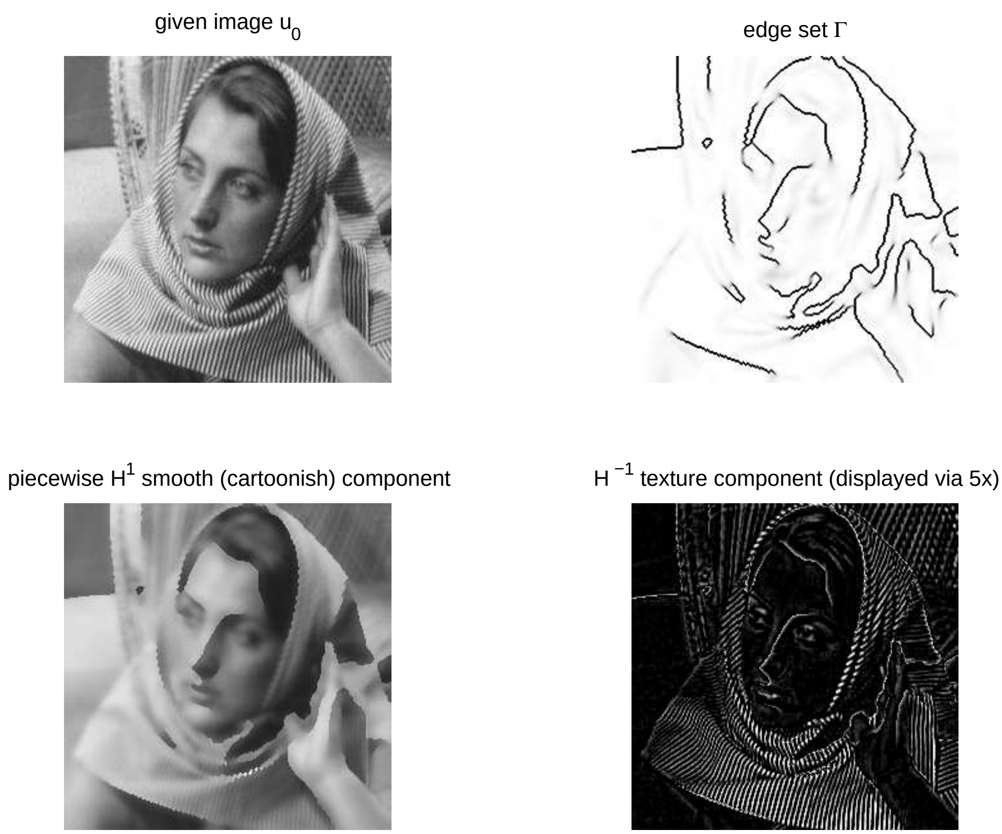

Figure 5: The computational result from Shen [39] confirms that natural H^{-1}-textures (on the lower right panel) do demonstrate the compositional characteristics of multiple beamlets, as theoretically predicted by the current work.

Acknowledgments

The author is grateful to the Institute of Mathematics and its Applications (IMA) at the University of Minnesota for her active roles in promoting this new area of mathematical image and vision analysis, as well as for the profound benefits the author has received from the workshops.

I dedicate this work to my dear former Ph.D. advisor Gil Strang for all his generous and kind care throughout the years, to both my research and my life in the USA. If Einstein's time machine could send me back for a decade, I would still choose Gil as my advisor for my research and life.

References

[1] L. Ambrosio. A compactness theorem for a new class of functions of bounded variation. *Bollettino U. M. I.*, 7(3-B):857–881, 1989.

[2] G. Aubert and P. Kornprobst. *Mathematical Problems in Image Processing.* Springer-Verlag, 2001.

[3] J.-F. Aujol, G. Aubert, L. Blanc-Feraud, and A. Chambolle. Image decomposition into a bounded variation component and an oscillating component. *J. Math. Imag. Vision*, 22(1):71–88, 2005.

[4] J.-F. Aujol and S.-H. Kang. Color image decomposition and restoration. *J. Visual Comm. Image Rep.,* to appear, 2005.

[5] A. Chambolle and P. L. Lions. Image recovery via Total Variational minimization and related problems. *Numer. Math.*, 76:167–188, 1997.

[6] T. F. Chan and J. Shen. On the role of the BV image model in image restoration. *Amer. Math. Soc. Contemporary Mathematics,* volume on *Recent Advances in Scientific Computing and Partial Differential Equations,* Editors: S. Y. Cheng, C.-W. Shu, and T. Tang, 330:25–41, 2003.

[7] T. F. Chan and J. Shen. *Image Processing and Analysis: variational, PDE, wavelet, and stochastic methods.* SIAM Publisher, Philadelphia, 2005.

[8] T. F. Chan and J. Shen. Variational image inpainting. *Comm. Pure Applied Math.*, 58:579–619, 2005.

[9] T. F. Chan, J. Shen, and L. Vese. Variational PDE models in image processing. *Notices Amer. Math. Soc.*, 50:14–26, 2003.

[10] I. Daubechies. *Ten lectures on wavelets.* SIAM, Philadelphia, 1992.

[11] I. Daubechies and G. Teschke. Variational image restoration by means of wavelets: Simultaneous decomposition, deblurring, and denoising. *Appl. Comput. Harmon. Anal.*, 19(1):1–16, 2005.

[12] R. A. DeVore, B. Jawerth, and B. J. Lucier. Image compression through wavelet transform coding. *IEEE Trans. Information Theory*, 38(2):719–746, 1992.

[13] D. L. Donoho. De-noising by soft-thresholding. *IEEE Trans. Information Theory*, 41(3):613–627, 1995.

[14] D. L. Donoho and X. Huo. Beamlets and multiscale image analysis. In *Multiscale and Multiresolution Methods*, volume 20 of *Lect. Notes Comput. Sci. Eng.*, pages 149–196. Springer, Berlin, 2002.

[15] D. L. Donoho and X. Huo. BeamLab and reproducible research. *Int'l J. Wavelets, Multiresolution, and Information Processing*, 2(4):391–414, 2004.

[16] D. L. Donoho and I. M. Johnstone. Ideal spacial adaption by wavelet shrinkage. *Biometrika*, 81:425–455, 1994.

[17] L. C. Evans. *Partial Differential Equations.* Amer. Math. Soc., 1998.

[18] D. J. Field. Scale-invariance and self-similar wavelet transforms: an analysis natural scenes and mammalian visual systems. In M. Farge, et al., editor, *Wavelets, Fractals and Fourier Transforms.* Oxford University Press, 1993.

[19] G. B. Folland. *Real Analysis - Modern Techniques and Their Applications.* John Wiley & Sons, Inc., second edition, 1999.

[20] S. Geman and D. Geman. Stochastic relaxation, Gibbs distributions, and the Bayesian restoration of images. *IEEE Trans. Pattern Anal. Machine Intell.*, 6:721–741, 1984.

[21] E. Giusti. *Minimal Surfaces and Functions of Bounded Variation.* Birkhäuser, Boston, 1984.

[22] G. Kanizsa. *Organization in Vision.* Praeger, New York, 1979.

[23] A. B. Lee, D. Mumford, and J. Huang. Occlusion models for natural images: a statistical study of a scale-invariant Dead Leaves Model. *Int'l J. Comp. Vision*, 41:35–59, 2001.

[24] E. H. Lieb and M. Loss. *Analysis.* Amer. Math. Soc., second edition, 2001.

[25] L. Lieu and L. Vese. Image restoration and decomposition via bounded total variation and negative Hilbert-Sobolev spaces. *UCLA CAM Tech. Report*, 05-33, 2005.

[26] F. H. Lin and X. P. Yang. *Geometric Measure Theory: An Introduction.* International Press, 2002.

[27] S. Mallat. *A Wavelet Tour of Signal Processing.* Academic Press, 1998.

[28] D. Marr. *Vision.* Freeman, San Francisco, 1980.

[29] Y. Meyer. *Oscillating Patterns in Image Processing and Nonlinear Evolution Equations*, volume 22 of *University Lecture Series.* AMS, Providence, 2001.

[30] J.-M. Morel and S. Solimini. *Variational Methods in Image Segmentation*, volume 14 of *Progress in Nonlinear Differential Equations and Their Applications.* Birkhäuser, Boston, 1995.

[31] D. Mumford and B. Gidas. Stochastic models for generic images. *Quaterly of Applied Mathematics*, 59:85–111, 2001.

[32] D. Mumford and J. Shah. Optimal approximations by piecewise smooth functions and associated variational problems. *Comm. Pure Applied. Math.*, 42:577–685, 1989.

[33] M. Nitzberg, D. Mumford, and T. Shiota. *Filtering, Segmentation, and Depth.* Lecture Notes in Comp. Sci., Vol. 662. Springer-Verlag, Berlin, 1993.

[34] S. Osher, A. Sole, and L. Vese. Image decomposition and restoration using total variation minimization and the H^{-1} norm. *Multiscale Model. Simul.*, 1:349–370, 2003.

[35] L. Rudin and S. Osher. Total variation based image restoration with free local constraints. *Proc. 1st IEEE ICIP*, 1:31–35, 1994.

[36] L. Rudin, S. Osher, and E. Fatemi. Nonlinear total variation based noise removal algorithms. *Physica D*, 60:259–268, 1992.

[37] J. Shen. Inpainting and the fundamental problem of image processing. *SIAM News*, 36, 2003.

[38] J. Shen. Bayesian video dejittering by BV image model. *SIAM J. Appl. Math.*, 64(5):1691–1708, 2004.

[39] J. Shen. Piecewise $H^{-1}+H^0+H^1$ images and the Mumford-Shah-Sobolev model for segmented image decomposition. *Appl. Math. Res. Exp.*, 4:143–167, 2005.

[40] J. Shen. Noncommutative monoids of occlusive preimages. *J. Math. Imag. Vision*, 24:5–17, 2006.

[41] J. Shen. A stochastic-variational model for soft Mumford-Shah segmentation. *Int'l J. Biomed. Imag.,* to appear, 2006.

[42] J. Shen and Y.-M. Jung. Weberized Mumford-Shah model with Bose-Einstein photon noise. *Appl. Math. Optim.,* in press, 2006.

[43] G. Strang and T. Nguyen. *Wavelets and Filter Banks.* Wellesley-Cambridge Press, Wellesley, MA, 1996.

[44] L. A. Vese. A study in the BV space of a denoising-deblurring variational problem. *Appl. Math. Optim.*, 44(2):131–161, 2001.

[45] S. C. Zhu and D. Mumford. Prior learning and Gibbs reaction-diffusion. *IEEE Trans. Pattern Anal. Machine Intell.*, 19(11):1236–1250, 1997.

[46] S. C. Zhu, Y. N. Wu, and D. Mumford. Minimax entropy principle and its applications to texture modeling. *Neural Computation*, 9:1627–1660, 1997.

[47] S. C. Zhu and A. Yuille. Region competition: unifying snakes, region growing, and Bayes/MDL for multi-band image segmentation. *IEEE Trans. Pattern Anal. Machine Intell.*, 18(9):884–900, 1996.